JOC The Journal of Organic Chemistry

Article

pubs.acs.org/joc

Synthesis and Comprehensive Structural and Chiroptical Characterization of Enones Derived from (−)-α-Santonin by Experiment and Theory

Marek Masnyk,[†] Aleksandra Butkiewicz,[†] Marcin Górecki,[†] Roman Luboradzki,[‡] Christoph Bannwarth,[§] Stefan Grimme,[*,§] and Jadwiga Frelek[*,†]

[†]Institute of Organic Chemistry, Polish Academy of Sciences, Kasprzaka 44/52, 01-224 Warsaw, Poland

[‡]Institute of Physical Chemistry, Polish Academy of Sciences, Kasprzaka 44/52, 01-224 Warsaw, Poland

[§]Mulliken Center for Theoretical Chemistry, Institute of Physical and Theoretical Chemistry, University of Bonn, Beringstr. 4, 53115 Bonn, Germany

Supporting Information

ABSTRACT: The aim of the present work is to explain the causes of the observed deviations from sector and helicity rules to determine the absolute configuration of optically active α,β-unsaturated ketones by means of electronic circular dichroism (ECD). To this end, a series of model compounds with a common decahydronaphthalene skeleton representing both *cisoid* and *transoid* enones were synthesized. In the framework of this work, detailed dichroic studies supported by single crystal X-ray analysis were performed where possible. To assist the achievement of the desired objectives the conformational flexibility of the selected *cis*-enones through the dependence of solvent and temperature on the ECD spectra were examined. All experimental studies were supplemented by detailed DFT calculations. A notable result of the study is assessing the applicability of the enone sector and helicity rules in dichroic studies and potential restrictions. To this end, a number of factors that could determine the signs of the individual Cotton effects has been considered. Among these nonminimum structure effects, i.e., twisting of the enone chromophore and nonplanarity of the enone double bond can be mentioned.

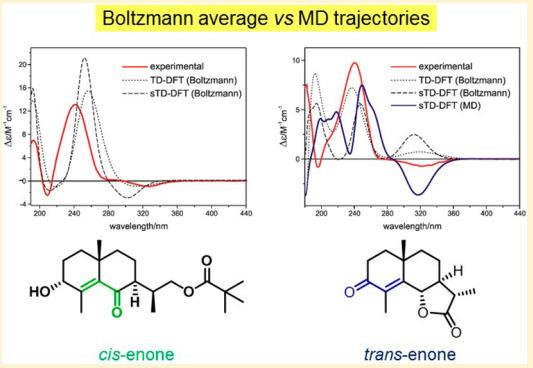

INTRODUCTION

The *cis*-enone chromophore is one of the most ubiquitous structural motifs in natural products. In particular, owing to their wide variety of biological activities, an important group of compounds is formed by α,β-unsaturated sesquiterpene ketones possessing the decahydronaphthalene skeleton form. Among them, eremophilane-type sesquiterpenes, represented in Chart 1 by (−)-eremophilone and (+)-fukinone, manifest selective antibacterial activity against Gram-positive organisms which are causes of human disease.[1,2] Moreover, the *Eremophila* species are constantly being considered the "number one medicine" by the Australian Aboriginal people due to their decongestant, expectorant, and analgesic properties.[3] The illudins, in turn, are a family of sesquiterpenes with antitumor and antibiotic properties produced by some mushrooms.[4] In Chart 1 this family is represented by (−)-illudin S.[5] The essential oil of the liverwort *Scapaniaundulata* contains a large variety of sesquiterpenes constituting important intermediates in the biosynthesis of functionalized sesquiterpenes. This group includes (−)-chiloscyphone[6] (Chart 1) which is the main component of the essential oil of the plant *Chiloscyphus polyanthus* (L) corda.

Many natural products exhibit desired biological effects only in one defined absolute configuration (AC). Therefore, the AC determination calls for methods allowing the stereochemical assignment in an unequivocal and straightforward way. For enones, one such basic method was, and still is, the analysis of their chiroptical properties. Extensive studies on this issue have led to a formulation of several rules linking the signs of Cotton effects (CEs) observed in the electronic circular dichroism spectra (ECD) with the absolute configuration of enones. At this point, the rules proposed in the 1960s by Djerassi et al.,[7] Whalley,[8] and Snatzke[9] should be mentioned. These rules were subsequently modified by Burgstahler and Barkhurst,[10] Kirk,[11]

Chart 1

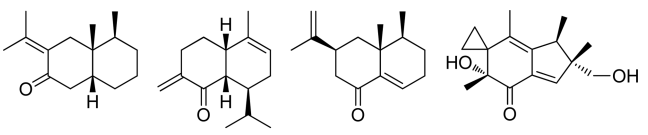

Received: February 25, 2016

DOI: 10.1021/acs.joc.6b00416
J. Org. Chem. XXXX, XXX, XXX−XXX

Chart 2

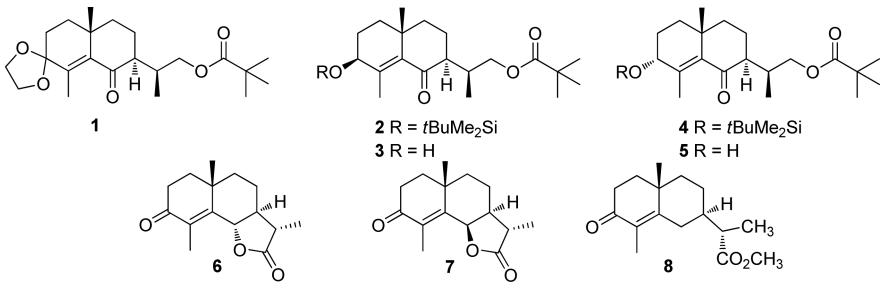

Scheme 1. Synthesis of 1

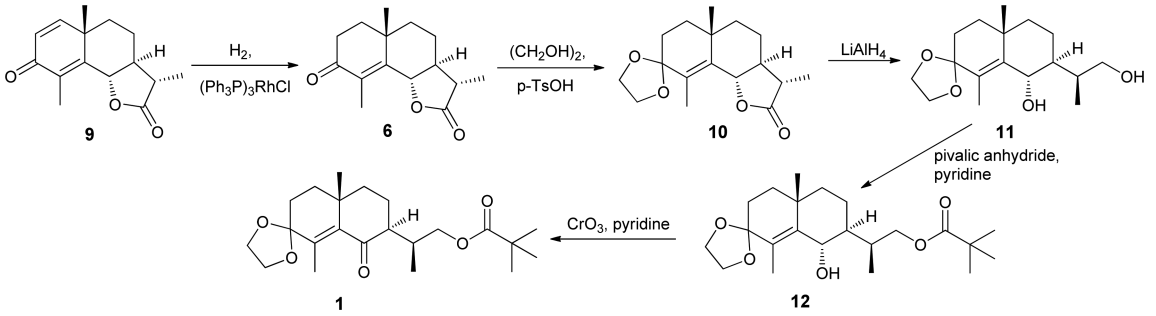

Gawronski,[12,13] and most recently by Kwit and Gawronski,[14,15] and Kuball et al.[16] As it turns out, the analysis of chiroptical properties of enones is quite complex due to many factors affecting respective CEs signs.[13] One of the most important of them is the multiplicity of conformational structures and small energy difference between them. Equally important is the correct description of electronic transitions involved in excitations that, particularly in a higher energy range, are not pure but are composed of multiple excitations on different chromophores present in the studied molecules. Recently, the impact of nonplanarity of the enone double bond on signs of particular CEs has additionally been demonstrated.[15,17] Nevertheless, for many enones the Kirk's orbital helicity rule[11] correlating the n → π^* CE sign with the helicity of the enone unit is working well.[11−13,18] However, we should draw attention to the fact that compared to *trans*-enones the *cisoid* enones have rarely been studied. Moreover, the relation between the helicity of the enone unit and its chiroptical properties appears to be more complex compared with their *trans* counterparts. Our preliminary study on this issue demonstrated derogations from the Kirk rule for certain *cis*-enones.[16,18−20] What results from these studies is that the nonsymmetrical conformation of the cyclohexanone ring causes a breakdown of the working orbital enone helicity rule.[16,20] These experimental observations, however, are not yet supported by either extended studies of other model compounds or an insightful theoretical examination.

Taking all this into consideration, we decided to carry out in-depth studies on the relationship between chiroptical properties and the structure of enones. To achieve this goal a number of suitable model compounds were synthesized and their geometries, structural parameters, and chiroptical properties were analyzed experimentally and theoretically. As model compounds for our chiroptical studies, a series of *cisoid* enones based on the decahydronaphthalene skeleton were selected (Chart 2). We recognized that (−)-α-santonin, a pharmaceutically important sesquiterpenoid, will be an excellent starting material for our synthetic endeavor due to its significant abundance and high functionality. Therefore, manipulating the structure of santonin toward the desired structures should proceed smoothly, efficiently, and according to the planned synthetic strategy. Moreover, chemical and microbial transformations of santonin into bioactive, potentially bioactive, or synthetically interesting products may also be relevant due to its relatively low price related to its abundance.

The choice of dihydrosantonin derivatives **1**−**5** was additionally motivated by their conformational flexibility and presence of substituents with their own interfering circular dichroic activity. Although these terpene enones are computationally more challenging compared to the previously studied steroidal enones,[16,18−20] their choice as models should enable a close examination of the influence of substituents in proximity to the chromophore on the conformation and thus their chiroptical properties. Finally, this set of molecules has been supplemented by representative *trans*-enones, i.e., dihydrosantonin (**6**), epidihydrosantonin (**7**), and its reduction product **8**. The idea behind this is to examine the viability of the orbital helicity rule based on the *cis*- and *trans*-enones that possess the same carbon framework. This should help in the interpretation of the obtained results and allow proper conclusions to be drawn on their basis. In the present study, we have considered substitution of cyclohexanone or cyclohexenone rings, respectively, in *cis*- and *trans*-enones due to the likelihood of opposing chiroptical effects.

We intend to achieve the planned goal by controlling the influence of conformational changes of the cyclohexanone and cyclohexenone rings on the diagnostic ECD bands. Our studies are focused on the band attributed to the enone n → π^* transition, occurring at ∼320 nm, since this particular band is subject to the enone helicity rule.[11] Moreover, this ECD band is clearly separated from the higher energy $\pi \rightarrow \pi^*$ band so that the risk of confusing overlap is minimized.

We decided to use ECD spectroscopy in tandem with time-dependent density functional theory (TDDFT) calculations.

DOI: 10.1021/acs.joc.6b00416
J. Org. Chem. XXXX, XXX, XXX−XXX

Scheme 2. Synthesis of 2 and 3

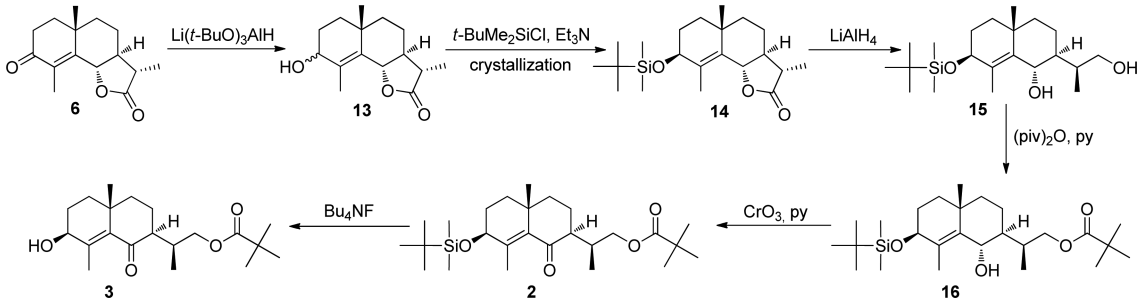

Scheme 3. Synthesis of 4 and 5

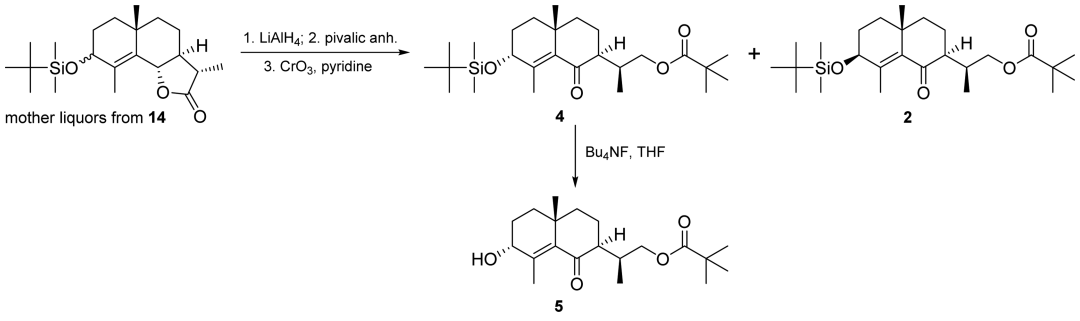

Scheme 4. Synthesis of 7 and 8

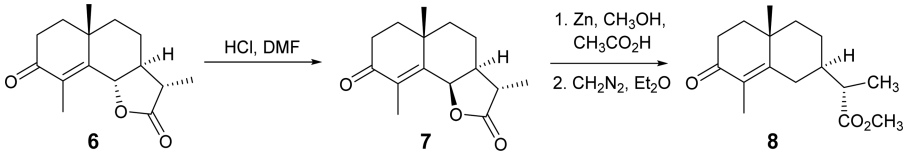

Currently, chiroptical methods combined with quantum chemical calculations are considered as the most powerful tools for elucidating stereochemistry and monitoring even the smallest changes in the geometry of chiral molecules. A combined experimental and theoretical analysis of ECD spectra has already proven useful and reliable in the determination of the absolute configuration of various classes of chiral molecules.[21−29]

It should be stressed that only properly assigned electronic transitions occurring within the enone chromophore and its immediate surroundings allow for rational stereochemical analysis.[14,15] Thus, we hope that the combined experimental and theoretical analysis will enable an explanation of the origin of discrepancy noted above in the working enone helicity rule. Henceforth, it should be possible to find determinants which influence both the sign and the magnitude of the Cotton effects strongly.

RESULTS AND DISCUSSION

1. Synthesis. Compound **1** was synthesized from natural (−)-α-santonin (**9**) according to Scheme 1. (−)-α-Santonin (**9**) was selectively hydrogenated over Wilkinson's catalyst producing dihydrosantonin[30,31](**6**), in which the carbonyl group was then subjected to a ketalization reaction with ethylene glycol in the presence of *p*-toluene sulfonic acid. The resulting ketal **10** was reduced with lithium aluminum hydride, and then the yielded diol **11** was selectively acylated with the pivalic anhydride in pyridine giving the monohydroxy alcohol **12**. Finally, the alcohol **12** was oxidized with chromium trioxide in pyridine yielding enone **1**.

Enones **2** and **3** were synthesized according to Scheme 2. Dihydrosantonin (**6**) was reduced with lithium tri-*tert*-butoxyaluminum hydride producing an inseparable mixture of stereomeric alcohols **13** in a ratio of 17:3 (equatorial:axial). The hydroxyl group in **13** was then protected as *tert*-butyldimethylsilyl ether in the reaction with *tert*-butyldimethylchlorosilane. Crystallization of the crude reaction product gave pure equatorial ether **14**, which was subsequently reduced to diol **15** with lithium aluminum hydride. The selective acylation of **15** with pivalic anhydride in pyridine provided monohydroxy alcohol **16**, which was converted into enone **2** by oxidation with chromium trioxide in pyridine. Cleavage of the silyl ether **2** with tetrabutylammonium fluoride yielded enone **3**.

Mother liquors remaining after crystallization of **14** were taken for further elaboration. The same reaction sequence as that for **16**−**3** (Scheme 2) yielded a separable mixture of epimeric sillyl ethers **4** and **2**. Deprotection of hydroxyl group in **4** yielded the axial alcohol **5** (Scheme 3).

Dihydrosantonin (**6**) was converted into dihydro-6-epi-santonin (**7**) by epimerization in DMF containing 5% anhydrous HCl according to a commonly used procedure in santonin chemistry (Scheme 4).[31−33] Treatment of compound **7** with zinc dust in methanol with glacial acetic acid caused reductive cleavage of the *cis*-fused lactone ring with formation of carboxylic acid which was then esterified with ethereal diazomethane yielding methyl ester **8**.[32,33]

DOI: 10.1021/acs.joc.6b00416
J. Org. Chem. XXXX, XXX, XXX−XXX

Interestingly, when dihydrosantonin (**6**) was subjected to rapid crystallization from a hot mixture of 1:1 methanol/water, plate-like crystals were obtained. In contrast, slow evaporation of methanol from the mother liquor that remained after separation of the plate-like crystals yielded needle-like crystals. In the asymmetric crystal unit of dihydrosantonin (**6**) there are two homohelical molecules with an enone torsion angle ω equal to −177.4° and −178.7° and a τ angle, defining the nonplanarity of the enone double bond, of −4.6° and −6.7°, respectively (for definition of angles ω and τ, see Chart 3).

Chart 3. Schematic Definition of Angles ω and τ

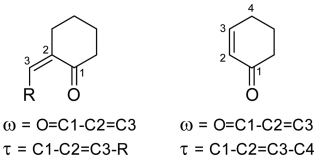

However, infrared spectra for both forms were identical in the range of measurement error. Moreover, the single crystal X-ray diffraction showed that despite the difference in morphology, both forms had the same unit cell (Figure 1). In light of these facts, the existence of two polymorphic forms is excluded.

For dihydroepisantonin (**7**), we were able to obtain two distinct crystal forms by crystallization from a mixture of methanol/water 1:1 and hexane. In the first case, needle-like crystals were obtained, while the second, where hexane was used as a solvent, yielded prismatic-shaped crystals (micrographs of the forms are shown in the Supporting Information (SI)). In the unit cell of the needle-like crystals of dihydroepisantonin (**7**) there are two molecules, one of which is homohelical and the other heterohelical. The enone torsion angle ω in the heterohelical molecule is equal to −169.0°, and the ene torsion angle τ, 3°. The ene torsion angle τ is defined as C/H−C═C−C(═O), where C/H is *syn* to the C−C(═O) bond (see Chart 3).[14,15] In the homohelical molecule the same angles are equal to +177.0° and +3.3°, respectively. On the other hand, the prismatic-shaped form contains only one molecule of dihydroepisantonin (**7**) in its unit cell with ω and τ angles equal to −170.0° and −1.4°, respectively.

These two forms of dihydroepisantonin (**7**) crystals differed both in the infrared spectra as well as in elementary cells (Experimental Section, Figures 1 and 2), thus demonstrating the existence of two polymorphic forms of **7** (see Supporting Information for X-ray details).

Experimental solid-state ECD spectra of both polymorphic forms of **7** recorded using integrating sphere attachment for a regular ECD spectrometer once again demonstrated the utility of diffuse transmittance CD (DTCD) using the pellet technique to distinguish polymorphs of a compound.[34,35] As can be seen in Figure 2, the spectra show significant differences, especially in the enone n → π^* transition spectral range. In this region, the Cotton effect of the prism form of **7** is bisignate while that of the needle form is monosignate and positive. Based on the X-ray data the difference in the conformation of the cyclohexanone ring in both polymorphic forms is also clearly visible, as can be seen in Figure 2.

2. Experimental and Calculated ECD Spectra of Enones 1−8. The experimental electronic absorption (EA) and ECD data of enones **1**−**8** are collected in Table 1.

The EA spectra of enones **1**−**8** display two well-resolved bands arising at around 320 and 240 nm. The intensity of bands occurring at ∼240 nm is much higher for *trans*-enones **6**−**8** than for their *cis* counterparts, as expected.[13] In turn, four bands within the spectral range of 185−360 nm are present in the ECD spectra, as can be seen in Table 1. The long-wavelength band occurring at ∼325 nm is attributed to the enone n → π^* transition, and the one arising in the range of 230−250 nm is assigned to the π → π^* excitation of the same chromophoric unit. The latter band corresponds to the EA band at ∼240 nm, and the former, to the long-wavelength band near 320 nm. In *trans*-enones **6**−**8**, at least in acetonitrile solution, the 320 nm ECD band exhibits a vibrational fine structure characteristic for enone carbonyls. There exists an inconsistency in the literature regarding the origin of the third band, appearing at *ca.* 200 nm which is practically undetectable in the UV spectra (see Table 1).[12,15,36] However, the latest results seem to promote the initial suggestion[12] that the sign of this CE in cyclic enones is controlled by the configuration of the saturated carbon−carbon chain.[15] The fourth electronic transition usually observed in the 185−195 nm range is considered to be an n → σ^* excitation.[11−13,36]

Regarding the spectral shape and CEs signs, the ECD spectra of compounds **1**−**6** and **8** show similar profiles with a negative n → π^* CE of comparable intensities of about $\Delta\varepsilon \approx 1$. The second ECD band at ∼240 nm, characterized by moderate to strong intensity (attributable to the π → π^* transition), is positive. The only exception in this regard is the enone **7** having both of these CEs of reverse signs with respect to enones **1**−**6** and **8**, including dihydrosantonin (**6**) and its reduction product **8** both representing *trans*-enones. For *trans*-enones **6** and **8**, in agreement with working orbital helicity rule,[11] a sign reversal of CEs with respect to the *cis*-enones **1**−**5** was expected to be the same as in the case of dihydroepisantonin (**7**).[11,12,15]

The obtained result means that the Kirk rule anticipating opposite signs for the two lowest-energy electronic transitions for the *cis*- and *trans*-enones does not apply here. However, the Kirk rule correlating a negative enone torsion angle with a

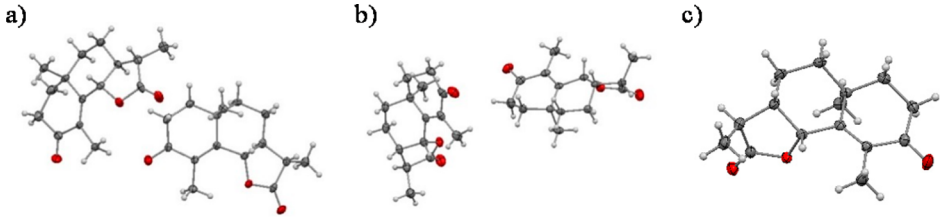

Figure 1. Molecular packing in crystals of the (a) dihydrosantonin (**6**, needles and plates), (b) dihydroepisantonin (**7**, needles), and (c) dihydroepisantonin (**7**, prism). The displacement ellipsoids are drawn at the 50% probability level.

DOI: 10.1021/acs.joc.6b00416
J. Org. Chem. XXXX, XXX, XXX−XXX

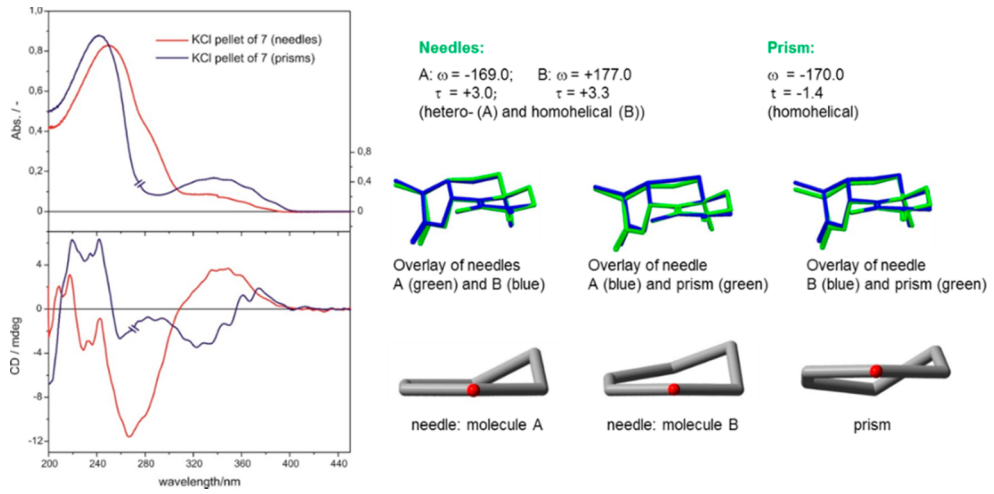

Figure 2. Left: Comparison of experimental ECD (bottom) and EA (top) spectra of needle and prism forms of enone **7** recorded in the solid state using KCl pellet technique in diffuse transmittance mode. Right-top: Overlay of enone **7** polymorphs crystallographic structures. Right-bottom: Solid-state conformation of cyclohexanone ring in prisms and needle crystal of **7**.

Table 1. EA and ECD Data for Enones 1−8 Recorded in Acetonitrile[a]

enone	UV [ε (λ_{max})]		ECD [$\Delta\varepsilon$ (λ_{max})]			
1	5020 (240.0)	55 (318.0)	+1.50 (187.0)	−2.17 (202.5)	+11.93 (238.5)	−1.12 (325.5)
2	5530 (246.0)	70 (317.5)	+6.50 (185.0)	−6.23 (206.0)	+9.74 (244.5)	−0.83 (325.5)
3	9870 (242.5)	60 (315.0)	+9.20 (186.5)	−5.80 (208.5)	+8.91 (245.0)	−0.61 (328.0)
4	5880 (242.5)	63 (314.0)	+9.18 (191.0)	−2.99 (210.0)	+18.09 (241.0)	−1.76 (323.5)
5	4570 (243.0)	54 (314.0)	+7.00 (193.0)	−2.51 (209.0)	+13.12 (241.5)	−0.95 (326.0)
6	14880 (242.5)	52 (319.5)	−0.81 (196.0)	+2.07 (209.5)[sh]	+9.75 (241.0)	−0.72 (321.0)[#]
7	14180 (243.5)	38 (330.0)	−6.63 (192.5)	+4.90 (215.5)	−4.75 (250.0)	+0.90 (350.5)
8	12980 (246.0)	50 (315.5)	−2.38 (194.0)	+3.00 (212.0)	+8.23 (244.0)	−0.64 (317.0)[†]

[a]EA and ECD values are given in M^{-1} cm^{-1} as ε ($\lambda_{max/nm}$) and $\Delta\varepsilon$ ($\lambda_{max/nm}$), respectively. sh: shoulder. #: an additional, very weak ($\Delta\varepsilon$ = +0.02) CE present at 376.0 nm. †: an additional, very weak ($\Delta\varepsilon$ = +0.04) CE present at 367.0 nm.

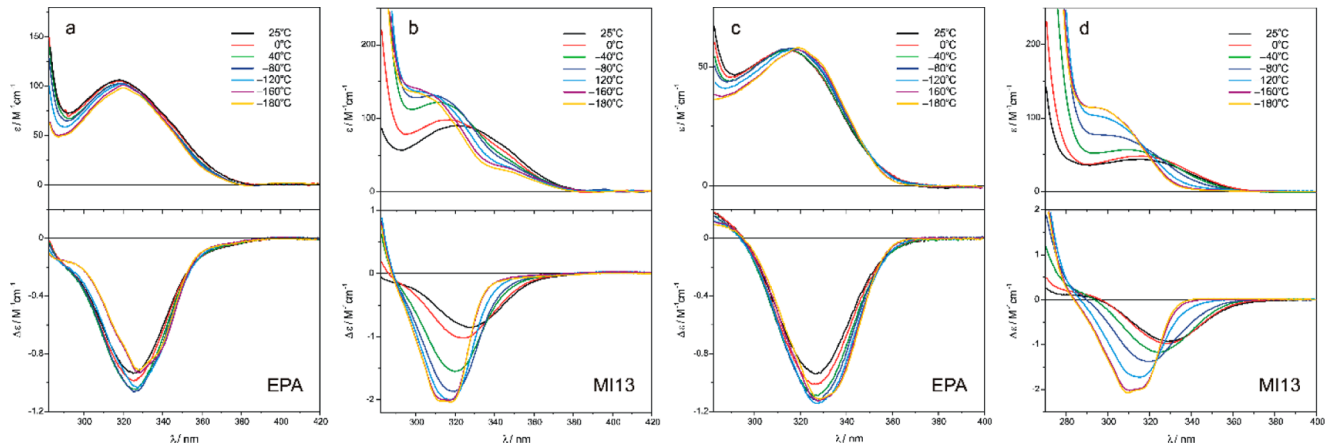

Figure 3. EA (top) and ECD (bottom) spectra of enones **3** (a, b) and **5** (c, d) recorded in EPA (Et_2O/isopentane/EtOH, 5:5:2, v/v) and MI13 (methylcyclohexane/isopentane, 1:3, v/v). The symbol ε denotes the molar decadic absorption coefficient; $\Delta\varepsilon$, the difference of the molar decadic absorption coefficients of left and right circularly polarized light; and λ, the wavelength. The lower temperature curves have been corrected for solvent contraction.

negative sign of the n → π^* CE and a positive sign of the π → π^* CE works perfectly for the examined *cis*-enones **1**−**5**.

Clarification of the inconsistency observed for the *trans*-enones **6** and **8** was expected in the evaluation of the experimental ECD spectra with respect to those predicted using reliable quantum chemical methods. A prerequisite of this task is to determine all conformers contributing significantly to the averaged spectra. Thus, the thorough conformational analysis guaranteeing obtainment of a reliable conformer population was conducted at the beginning. An in-depth analysis of the combined experimental and theoretical results separately for *cis*- and *trans*-enones is subject to the following considerations. Details about the conformational analysis, optimization, and reoptimization of results as well as simulation of EA and ECD spectra are contained in the section "Computational Details" directly following the "Experimental Section".

DOI: 10.1021/acs.joc.6b00416
J. Org. Chem. XXXX, XXX, XXX−XXX

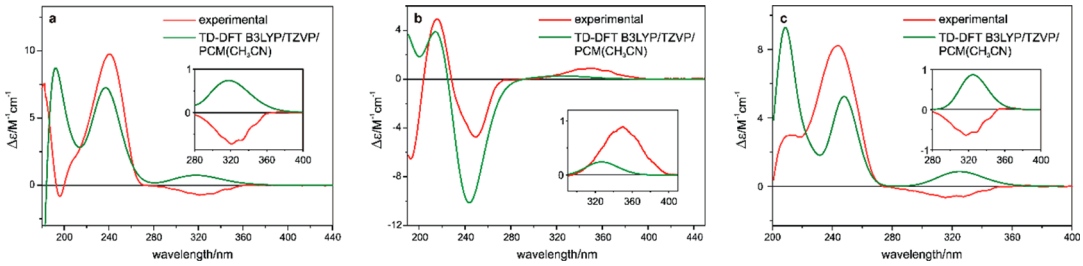

Figure 4. Comparison of computed ECD spectra of enones **6** (a), **7** (b), and **8** (c) obtained as a population weighted sum of the calculated spectra of individual conformers with experimental spectra recorded in CH_3CN. Inserts show the range of n → π^* transition.

*2.1. Chiroptical Properties of cis-Enones **1**–**5**.* Experimental and calculated electronic absorption spectra of *cis*-enones **1**–**5** are consistent regarding the position of absorption bands and their intensity. The comparison shows that the position of the $\pi \rightarrow \pi^*$ absorption bands in the calculated spectra required only a slight red shift of about 3 nm or no adjustment at all (see SI). After ensuring proper compatibility between experimental and calculated EA spectra, we proceeded to compare their ECD spectra. As seen in Figures S1–S5, the Boltzmann weighted ECD spectra for all the *cis*-enones under question reflect the experimental ECD features very well. The negative n → π^* CE is reproduced in the calculations for all five enones **1**–**5**. Consistently, the positive $\pi \rightarrow \pi^*$ CE at ∼240 nm is also reflected correctly as to the location and intensity. Similarly, the good agreement applies to the short-wavelength part of the spectrum regardless of the substituent type and the position of substitution in the skeleton. The data indicate that the *M* helicity of the enone chromophore in *cis*-enones **1**–**5** has a decisive impact on their chiroptical properties. This statement is confirmed by the same half-chair and chair conformation of rings A and B, respectively, in all conformers found (see Table S1 in Supporting Information). Also, the presence of a polar substituent such as a hydroxyl group at the C3 carbon atom in enones **3** and **5** affects neither the ECD curve shape nor the signs of the respective CEs. The electronic transition associated with the presence of this group in the experimental spectrum is hidden within the adjacent bands and can be attributed to the $n_{OH} - \pi_{C=O}^*$ type. At this point it should be added that not all conformers of enones **2**–**5** fulfill the Beecham's postulate of compliance between the helical turn of the four-atom helix containing allylic oxygen O–C–C(4)═C(5) and the sign of the $\pi \rightarrow \pi^*$ band CE of the enone chromophore (see Supporting Information).[37]

To strengthen the conclusions regarding the conformational homogeneity of the A and B rings in compounds **1**–**5**, the measurements of ECD spectra at variable temperatures were recorded for the enones **3** and **5** serving as representative model compounds (Figure 3). The results obtained in a nonpolar solvent MI13 (methylcyclohexane/isopentane, 1:3, v/v) at temperatures ranging from +25 °C to −180 °C show more than a 2-fold increase in the intensity of the n → π^* band combined with its shift toward higher energies of 15 and 19 nm for **3** and **5**, respectively. In contrast, lowering the temperature results in almost no changes in the band position and a barely perceptible increase in the intensity in a polar solvent (EPA: Et_2O/isopentane/EtOH, 5:5:2, v/v). The EPA result indicates the conformational homogeneity of the rings containing the enone chromophore without the need to stabilize them through intermolecular hydrogen bonding. In the MI13 case, however, lowering the temperature causes progressive elimination of high-energy conformers from the equilibrium and shifts it toward more stable conformers. With a decreasing temperature shift in the λ_{max} of the n → π^* CEs, i.e., $\Delta\lambda_{max}$, in MI13 is equal to 16 nm for enone **3** and 19 nm for enone **5**, thus approaching a value close to the electronic absorption at room temperature, i.e. 316 and 319 nm, respectively. The same $\Delta\lambda_{max}$ in EPA accounts to 3 and 2 nm respectively for enones **3** and **5**. This appears to be a case of the strong influence of the solvent, which likely manifests itself in either stabilization or destabilization of the investigated structures. Solvent polarity affects the electronic structure of the solute by, e.g., enabling or not the formation of intermolecular hydrogen bonds between the OH group and carbonyl of the enone unit or ester group. As a result, in the nonpolar solvent, the identity of the chromophore is changed due to the creation of associates. Thus, the presence of different molecular species leading to various behaviors must be considered in nonpolar and polar solvents.

To summarize this portion, it can be stated that the ECD spectra of *cis*-enones in solution studied here show similar profiles and all follow the Kirk enone helicity rule. This means that the sign and magnitude of the n → π^* CE are mainly determined by the helicity of the enone unit, i.e., the sign of the C═C–C═O (ω) angle. It implies that substituents at the C-3 position have a limited influence on ring conformation and thus a negligible effect on the ECD curves within compounds **1**–**5**.

*2.2. Chiroptical Properties of trans-Enones **6**–**8**.* As already mentioned previously, the *trans*-enones **6**–**8** behave differently with respect to their *cis* counterparts **1**–**5**. In enone **7**, the sign of the n → π^* CE is positive in agreement with the Kirk rule while a negative sign of the same CE in enones **6** and **8** violates this rule. On the other hand, simulated spectra of **6** and **8** calculated at the same level of theory as *cis*-enones **1**–**5** show positive n → π^* CEs, thus being in disagreement with the experiment but consistent with the rule (Figure 4).

The lack of agreement between experimental and theoretical spectra can be caused by multiple factors. One reason is the small difference in energy between conformers strongly associated with conformational flexibility. However, in the case of the investigated *trans*-enones only compound **8** exhibits a higher conformational flexibility closely related to mobility of the side chain attached to the C7 carbon atom. In this case, however, the 12 conformers found in the 3 kcal/mol window showed no significant differences in the bicyclic skeleton including the enone chromophoric unit. The other two *trans*-enones, i.e., **6** and **7**, are conformationally rigid as confirmed by the presence of only two conformers in the 3 kcal/mol energy range in both cases. Thus, the conformational flexibility cannot be the primary cause of the observed discrepancies.

DOI: 10.1021/acs.joc.6b00416
J. Org. Chem. XXXX, XXX, XXX–XXX

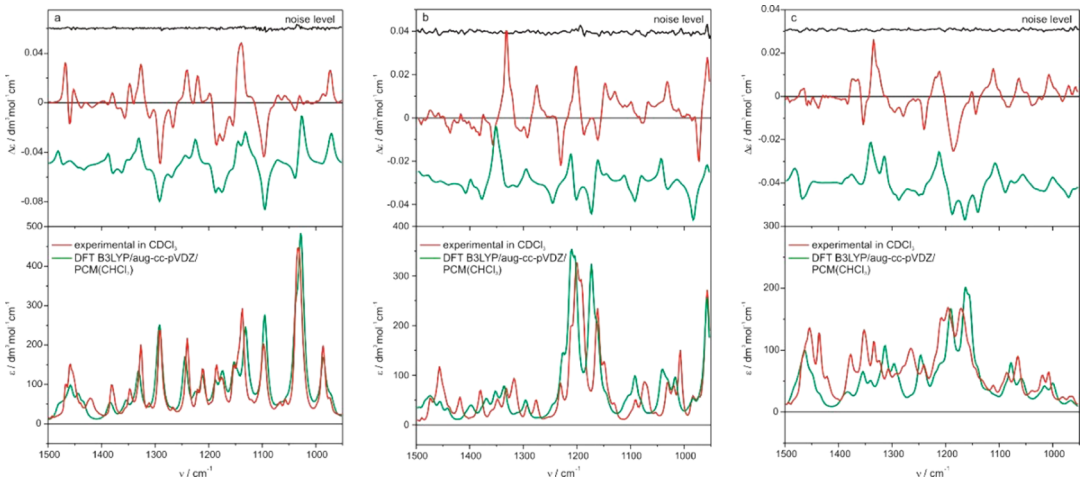

Figure 5. Experimental and calculated VCD spectra of enones **6** (a), **7** (b), and **8** (c). The simulated spectra were averaged with the Boltzmann distribution at PW6B95-D3/def2-QZVP+COSMO-RS level of theory (see computational details below).

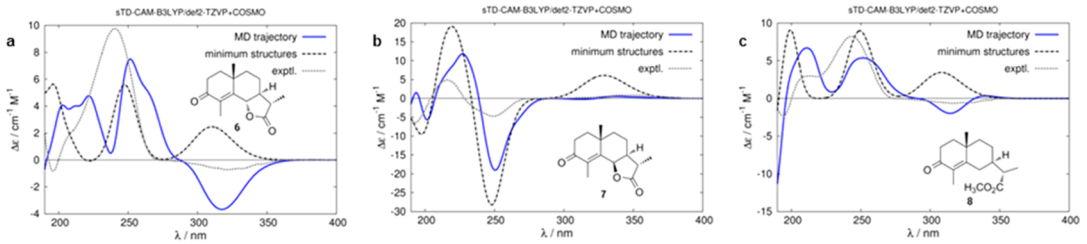

Figure 6. ECD spectra of *trans*-enones **6**, **7**, and **8** (a, b, and c, respectively). The experimental spectra (dashed gray) are recorded in acetonitrile. The computed spectra (blue solid lines) are obtained with sTD-DFT at the CAM-B3LYP/def2-TZVP+COSMO level on 100 MD "snap shots" (400 for compound **8**). The corresponding spectra obtained on Boltzmann-weighted minimum structures at the same level of theory are given as well (black dashed lines). All computed spectra are red-shifted by 0.5 eV.

Another limiting factor that may cause the theory mismatch with the experiment can be linked to disregard in the calculation of vibronic contributions, negligence of nonplanarity of the enone double bond, or the presence of polar substituents.[14−16,20] The presence of substituents in the chromophore vicinity introduces additional complexity to the geometric and electronic features of the compounds studied thus increasing their conformational flexibility and finally affecting their chiroptical properties. Such impact is seen in the case of dihydrosantonin (**6**) and dihydroepisantonin (**7**), i.e., molecules whose conformational mobility is very limited. In these cases, the difference of the AC at the C6 carbon atom induces a significant difference in the shape of the ECD curve. The signs of the experimental n → π^* and π →π^* bands are opposite although the geometry of the enone itself is the same.

To further ascertain the correctness of the conformational analysis, for the same set of conformers, the VCD spectra were calculated at the B3LYP/aug-cc-pVDZ/PCM($CHCl_3$) level of theory and compared with the experimental ones. As can be seen in Figure 5, the agreement between simulated and experimental spectra is excellent in all three cases. Thus, we received further support for the correctness of our conformational analysis, namely selecting all conformers contributing to the net ECD/VCD spectra.

In enones **6**−**8** the ECD bands within the n → π^* transition are highly structured, showing several identifiable bands assigned to vibrational progressions in the carbonyl stretching mode with the CE maxima at ∼320 nm for **6** and **8** and ∼350 nm for **7**. The spectra of enones **6** and **8** additionally exhibit a very weak positive band on a long wavelength part of this band, i.e. at 376 and 367 nm, respectively. This additional band, present in many spectra of the enones, was first remarked on by Kuball et al. and termed the "preband".[38−40] Based on the results of the extensive study of anisotropic circular dichroism (ACD) with enones as model compounds, they concluded that the sector and helicity rules can be used effectively provided that vibronic progressions of all possible conformers will be considered.[18,19,40] Otherwise, a different vibronic coupling caused by a variation in the surroundings of the chromophore may even induce the CE sign change. They have also stated that the enone helicity corresponds to the sign of the long wavelength part of the n → π^* CE.[16,40] Such compliance is observed in enones **6** and **8** in which the preband CE is positive thus being in agreement with the Kirk rule.

Among the limiting factors, one should also take into account the impact of the applied level of theory on compliance with the experiment. Significant deviations between the methods used appear to be particularly common for inherently achiral chromophores. It is already known that even moderate changes in the calculation level may lead to a sign change, thus resulting in unreliable theoretical predictions.[17,41,42]

We, therefore, extended our computational study of the ECD spectra to gain more insight. For this purpose, we reoptimized the structures by the efficient, dispersion-inclusive PBEh-3c level and recomputed the Boltzmann weights (for details see Computational Details). Then the recently proposed simplified time-dependent density functional (sTD-DFT) approach on a CAM-B3LYP/def2-TZVP reference was used to compute the

DOI: 10.1021/acs.joc.6b00416
J. Org. Chem. XXXX, XXX, XXX−XXX

absorption and ECD spectra of all compounds. The calculation has been conducted in the gas phase as well as by applying the implicit conductor-like-screening solvation model COSMO in the ground state. For the *cis*-enones, it can be seen that the agreement between the experiment and the sTD-DFT results is very good for both the EA and the ECD spectra (see SI).

Furthermore, we observed good mutual agreement with the previous calculations at the B3LYP level. The influence of COSMO is negligible for the *cis*-enones. In these cases, all experimental ECD bands are computed with the correct sign. From Figure 6 one can see that this does not hold for the *trans*-enones. While the ECD signal of the $\pi \rightarrow \pi^*$ transition (around 250 nm) is the same in the gas phase and with COSMO, this does not hold at all for the $n \rightarrow \pi^*$. In the gas phase, this band is predicted to be negative in sign for all *trans*-enones **6**–**8**. When the solvation model COSMO is used, the sign of this band is reversed in all these cases. This is in agreement with the computed spectra mentioned above (Figure 4) where a continuum solvation model (PCM in that case) was used as well. One can infer that the implicit solvation leads to a different stabilization of partial charges (and orbitals) which in turn changes the coupling in the excited state. Although this seems to be a realistic situation in solution, a positive sign for this ECD band (as it is present when COSMO is used) is experimentally observed only for dihydroepisantonin (**7**). It was mentioned above that the ECD of the $n \rightarrow \pi^*$ transitions seems to feature some fine structure and, thus, might not sufficiently be described solely by minimum geometries. For the "problematic" *trans*-enones **6**–**8**, we therefore chose to compute ECD spectra on snap shots of a molecular dynamics simulation (MD; see Computational Details). Thus, non-minimum geometry effects on the ECD spectra can be taken into account (Figure 6).

It is nicely observed that this improves the agreement with the experimental spectra for all compounds. While the $n \rightarrow \pi^*$ turns out to be entirely negative for dihydrosantonin (**6**), it remains (weakly) positive for dihydroepisantonin (**7**). The corresponding ECD signal in compound **8** shows both a small positive feature to lower energies and a stronger negative one to those slightly above. It can be assumed that longer MD runs will further improve the agreement between simulated and measured spectra. At this moment, it is stated that by including structures from MD runs (i.e., by going beyond the minimum structure approach), the differences in the $n \rightarrow \pi^*$ bands of the *trans*-enones **6**–**8** are captured correctly. Note that averaging UV or ECD spectra along MD trajectories does not yield the vibronic fine structures of absorption and ECD bands, as these result from a quantum mechanical effect[43] which is not properly captured by computing vertical excitations obtained from a classical MD.

While all minimum structure approaches were successful in predicting the sign of the $\pi \rightarrow \pi^*$ band, none of the considered minimum geometry approaches can yield the right sign of the $n \rightarrow \pi^*$ band for all *trans*-enones. To achieve this, one has to go beyond the minimum structure approximation in the calculation of ECD spectra, as we have done by computing ECD spectra on an MD trajectory. The agreement observed with minimum structure based approaches (see, e.g., ECD spectra of **6** and **8** in the SI) without an implicit solvation model has to be interpreted as fortuitous error cancellation. It has to be added at this point that a cross check calculation for compound **5**, used as a representative model of *cis*-enones, shows no changes in sign compared to the minimum structures (see SI, p 185). This result strengthens the observation that the ECD of the *cis*-enones is more robust than the one of the *trans*-enones.

CONCLUSIONS

As a part of our ongoing research on the structure–chiroptical properties relationship of α,β-unsaturated ketones, we describe here a detailed stereochemical analysis of a set of model compounds synthesized from (−)-α-santonin as a substrate. The geometries, structural parameters, and chiroptical properties of all models were analyzed experimentally and theoretically in detail by electronic circular dichroism (ECD) partially supported by vibrational circular dichroism (VCD). The structural characterization was assisted by nuclear magnetic resonance (NMR) and single crystal X-ray analysis where possible. In the case of dihydroepisantonin (**7**) we identified and characterized the two polymorphic forms that are also distinguishable by solid-state ECD.

We have furthermore shown that the sign of the $n \rightarrow \pi^*$ ECD signals in *trans*-enones is not sufficiently described by a minimum structure model. In such cases, it seems to be necessary to go beyond this approach. We have achieved this by computing ECD spectra on snap shots from a molecular dynamics simulation. Thus, we demonstrated the remarkable utility of the combined experimental and theoretical chiroptical analysis to provide the complete three-dimensional solution structures of chiral enones. Application of state-of-the-art theoretical analysis allowed extraction of structural information from the plethora of structure-sensitive bands in α,β-unsaturated ketones.

EXPERIMENTAL SECTION

General Techniques. Commercial reagents of the highest purity available were used without further purification. All reactions were monitored by thin-layer chromatography using aluminum backed silica gel plates 60 F_{254}; visualization was accomplished with UV light and/or staining with 50% H_2SO_4. Standard flash chromatography procedures were followed (using silica gel with particle size 40–63 μm). The melting points are given without correction. Optical rotation was measured on a digital polarimeter at ambient temperature and are quoted in units of 10^{-1} deg cm^2 g^{-1}. IR spectra were measured for samples as KBr pellets or films or examined directly in the solid or liquid state without further preparation with universal Attenuated Total Reflectance (ATR) accessory in an FT-IR spectrophotometer. ^{1}H NMR and ^{13}C NMR spectra were recorded in Fourier transform mode at the field strength specified on a 400 or 500 MHz spectrometer using $CDCl_3$ as solvent and TMS as internal standard and are reported as δ values (ppm) relative to residual $CHCl_3$ signal δH (7.26 ppm) and $CDCl_3$ δC (77.16 ppm) as internal standards, respectively. Mass spectra were obtained at 70 eV. Electrospray ionization (ESI) mass spectrometry (MS) experiments were performed on a mass spectrometer under normal conditions. PFK solution was used as a calibrant for HRMS measurements. UV spectra were measured using acetonitrile as a solvent. The ECD spectra of **1**–**8** were recorded between 450 and 180 nm at room temperature in spectroscopic grade acetonitrile with concentrations in the range from 3.0×10^{-4} to 7.47×10^{-4} M in a quartz cell with a path length of 0.1, 0.2, 0.5, 1, or 2 cm. All spectra were recorded using a 100 nm/min scanning speed, a step size of 0.2 nm, a bandwidth of 1 nm, a response time of 0.5 s, and an accumulation of 5 scans. The spectra were background corrected.

Low-temperature ECD measurements of **3** were performed in the temperature range 298–93 K in a solution of MI13 (methylcyclohexane/isopentane, 1:3, by vol.) and EPA (Et_2O/isopentane/EtOH, 5:5:2, by vol.) as solvents. The solutions with concentrations in the range from 1.82×10^{-3} to 1.87×10^{-4} M were measured between 450

DOI: 10.1021/acs.joc.6b00416
J. Org. Chem. XXXX, XXX, XXX–XXX

and 260 nm in a 1 cm quartz cell. Baseline correction was achieved by subtracting the spectrum of a reference solvent obtained under the same conditions. All spectra were normalized to $\Delta\varepsilon$ using volume correction for EPA and MI13.

The ECD solid-state spectra of two polymorphic forms of **7** were obtained using Diffused Transmission (DTCD) mode as the KCl pellet was placed in the integrating sphere coated with barium sulfate and introduced to the high sensitivity photomultiplier tube situated at 90°. ECD spectrum (0.164−1.006 mg/100 mg KCl) was recorded between 400 and 200 nm at room temperature using the following parameters: a 100 nm/min scanning speed, a step size of 0.2 nm, a bandwidth of 5 nm, a response time of 0.5 s, and an accumulation of 5 scans. The resulting spectrum was background corrected. The KCl pellet was mounted on a rotatable holder located just before integrating sphere. The sample was measured upon rotation of the disk around the incident axis direction at various rotation angles. The spectra were almost identical, demonstrating the absence of detectable spectral artifacts. Linear dichroism (LD) was also measured; the order was less than 2×10^{-3} OD.

The VCD and IR spectra of **6**−**8** were measured at a resolution of 4 cm^{-1} in $CDCl_3$. The FT-VCD spectrometer was equipped with dual sources and dual PEM (PhotoElastic Modulator). Solutions with molar concentrations of 0.14 [**6** (6.08 mg) in $CDCl_3$ (180 μL)], 0.20 [**7** (8.39 mg) in $CDCl_3$ (180 μL)], and 0.21 [**8** (9.996 mg) in CDCl3 (180 μL)], were measured in a BaF_2 cell with a path length of 99.8 μm. The ZnSe photoelastic modulator was set to 1400 cm^{-1}. The spectra were measured for 3 h 30 min (10240 scans). Baseline correction was achieved by subtracting the spectrum of a reference sample of $CDCl_3$ recorded under the same conditions as the enones samples. Single crystal X-ray diffraction measurements for **1**, **3**, **6**, and **7** (needles and prism-like crystals) were carried out at 100 K with graphite monochromated Cu Kα radiation (1.54184 Δ). All non-hydrogen atoms were refined as anisotropic while hydrogen atoms were placed in calculated positions and refined in riding mode. Crystallographic data for **1**, **3**, **6**, and **7** reported here have been deposited with the Cambridge Crystallographic Data Centre (Deposition Nos. CCDC 1426351 for **1**, 1428736 for **3**, 1428735 for **6**, and 1428737 as well as 1428889 for **7** (prism-like and needle-like crystals, respectively). These data can be obtained free of charge via www.ccdc.cam.ac.uk/data_request/cif.

COMPUTATIONAL DETAILS

In the case of *cis*-enones **1**−**5**, a conformational search on the molecular mechanics level was carried out within a 10 kcal/mol energy window using CONFLEX 7[44] software with the MMFF94s force field (a static variant of MMFF94). Depending on the compound, we obtained 237 to 535 conformers (detailed data in the Supporting Information = SI). To reduce the number of conformers and to remove conformers not fitting within the narrower 5 kcal/mol energy window, the structures were optimized using the same force field. This additional optimization resulted in a much-reduced number of structures, namely 55 to 129 depending on the compound (see SI). Next, the obtained geometries were subsequently reoptimized using the density functional theory (DFT) employing Gaussian09[45] at the B3LYP/TZVP/PCM(CH_3CN) level (see SI). As a result, 10 to 25 structures with a population of more than 1% were obtained and later used to simulate chiroptical properties (see SI).The EA and ECD spectra of all conformers were calculated by the TDDFT method with the TZVP basis set and B3LYP functional by applying the PCM model to reflect solvent influence. Next, before comparing the predicted and experimental ECD spectra, the agreement of experimental and calculated EA spectra was verified, as their conformity is a prerequisite for analyzing the corresponding ECD spectra.[46]

The geometries were reoptimized at the PBEh-3c level,[47] i.e., employing a hybrid density functional in combination with a double-ζ basis set and the atom-pairwise D3(BJ) dispersion[48,49] and geometrical counterpoise (gCP)[50] corrections. This composite method yields highly accurate geometries for organic compounds at comparably low cost. The TURBOMOLE suite of programs (version 7.0)[51,52] has been used for this purpose (employing the numerical quadrature grid *m4*). Harmonic frequencies were computed at this level as well to verify these structures as minima.

In order to obtain free energies for each conformer, electronic energies ($E_{el.}$, including nuclear repulsion and London dispersion) were computed with the D3(BJ) dispersion-corrected PW6B95[53] functional (grid *m5*) and Ahlrichs' def2-QZVP basis set[54,55] on the PBEh-3c geometries. The ro-vibrational contributions (G_{RRHO}) to the free energy (including the zero-point vibrational energy) were computed according to ref S6 using the scaled (by a factor of 0.95) harmonic frequencies at the PBEh-3c level of theory. Solvent effects to the free energy ($\delta G_{solv.}$) were accounted for by the COSMO-RS method employing the 2012 parametrization for acetonitrile.[57−59] The resolution-of-identity approximation for the Coulomb integrals (RI-J) was applied in all TURBOMOLE calculations using a matching default auxiliary basis.[60,61] The relative free energies between the conformers are then given as the sum of the individual contributions:

$$\Delta G = \Delta E_{el.} + \Delta G_{RRHO} + \Delta\delta G_{solv.}$$

The Boltzmann weights were calculated using the free energies which were computed as described above.

For each conformer, single-point calculations on the PBEh-3c geometries were performed with the range-separated hybrid density functional CAM-B3LYP[62−65] (numerical quadrature *grid5*) and the def2-TZVP[55,66] basis set. Based on this ground state, all singly excited states up to 10 eV were computed with the simplified time-dependent density functional theory (sTD-DFT) approach.[67−69] A development version of the ORCA program[70,71] has been used for this purpose. The same procedure was repeated but including the COSMO solvation model (ε = 35.688).[72]

For the computations on an MD trajectory, a quantum mechanically derived force field[73] was parametrized using the PBEh-3c Hessian (matrix elements scaled 0.95) of the most stable conformer of **6** and **7**. For compound **8**, the four most stable conformers were considered.

With the resulting force fields, a molecular dynamics simulation (NPT conditions) was performed of one molecule dissolved in a box of 200 acetonitrile molecules at 300 K (periodic boundary conditions were employed). After equilibrating for 0.5 ns, we ran the simulation for another 0.5 ns with a time step of 1 fs. The X−H bonds were kept fixed using the SHAKE[74,75] algorithm. The QMSIM[76] program has been used for this purpose. Every 5 ps, a structure was extracted (100 in total for each considered starting conformer) and an sTD-CAM-B3LYP/def2-TZVP+COSMO calculation was performed on the resulting solute geometry. For compound **8**, the resulting spectra were weighted by the Boltzmann weights of the respective starting conformers.

The molar extinction (ε) and circular dichroism ($\Delta\varepsilon$) spectra were simulated by convoluting the oscillator and rotatory strengths, respectively, with Gaussian functions with a full width at 1/e maximum of 0.5 eV (0.3 eV for calculations on MD trajectories). All spectra are shifted by −0.5 eV (i.e., red-shifted) to match the experimental intense absorption band around 250 nm. The dipole length formalism has been used for the oscillator strengths while the origin-independent dipole velocity form was used for the rotatory strengths.

Preparation of Dihydrosantonin 6. Tris(triphenylphosphine)-rhodium(I) chloride (280 mg, 0.3 mmol) was dissolved in acetone (50 mL) in a hydrogenation apparatus which was then flushed three times with hydrogen. After stirring the solution in an atmosphere of hydrogen for about 1 h the hydrogen uptake ceased and constant pressure was attained. Then a solution of (−)-α-santonin (**9**, 600 mg, 2.4 mmol) in acetone (25 mL) was added, and the stirring was continued until hydrogen consumption ceased. The solvent was evaporated to dryness, and the residue was chromatographed (20% ethyl acetate in hexanes) giving **6** (595 mg, 97%).

Colorless crystals, mp 100−101 °C (lit. 100−102,[30] 102,[31] 101−102[77] °C); $[\alpha]_D^{24}$ +72 (*c* 0.5, EtOH) [lit.[77] $[\alpha]_D$ +79 (*c* 1.42)]; ^{1}H NMR (500 MHz, $CDCl_3$): δ = 4.69 (dd, *J* = 11.6, 1.3 Hz, 1H), 2.54 (ddd, *J* = 16.7, 14.1, 5.0 Hz, 1H), 2.44 (dt, *J* = 16.7, 4.3 Hz, 1H), 2.35 (dq, *J* = 12.2, 6.9 Hz, 1H), 2.02−1.97 (m, 1H), 2.00 (s, 3H), 1.96−

DOI: 10.1021/acs.joc.6b00416
J. Org. Chem. XXXX, XXX, XXX−XXX

1.87 (m, 2H), 1.81 (dt, J = 13.4, 4.6 Hz, 1H), 1.77−1.63 (m, 2H), 1.56 (td, J = 13.2, 4.4 Hz, 1H), 1.34 (s, 3H), 1.27 (d, J = 6.9 Hz, 3H); ^{13}C NMR (125 MHz, $CDCl_3$): δ = 198.8, 177.6, 152.5, 128.55, 81.9, 52.9, 41.7, 41.2, 38.3, 38.2, 33.6, 24.6, 24.2, 12.4, 11.2; IR ($CHCl_3$): 2937, 1779, 1668, 1622, 1458, 1327, 1138, 1033 cm^{-1}; Anal. Calcd for $C_{15}H_{20}O_3$: C, 72.55; H, 8.12. Found: C, 72.64; H, 8.03.

Fast crystallization of dihydrosantonin (**6**) from the hot mixture of methanol/water 1:1 led to plate-like crystals, 100−101 °C, IR (KBr): 2940, 1875, 1792, 1767, 1675, 1623, 1455, 1331, 1292, 1238, 1209, 1185, 1138, 1099, 1028, 985 cm^{-1}.

Slow evaporation of the methanol from the mother liquor remained after separation plate crystals gave needle-like crystals: mp 100−101 °C; IR (KBr): 2940, 1874, 792, 1767, 1675, 1622, 1454, 1331, 1291, 1238, 1209, 1185, 1138, 1099, 1028, 985 cm^{-1}.

Preparation of Ketal 10. A boiling mixture of dihydrosantonin (**6**, 710 mg, 2.9 mmol), benzene (50 mL), *p*-toluenesulfonic acid monohydrate (40 mg, 0.2 mmol), and ethylene glycol (1.5 mL) was distilled slowly through a small Vigreux column for a period of 5 h (10 mL of distillate was collected). The cooled reaction mixture was washed with aqueous sodium bicarbonate, and the organic layer was dried over Na_2SO_4 and evaporated to dryness. The main product of the reaction 10 (460 mg, 55%) was isolated by chromatography (5% acetone in hexanes).

Colorless crystals, mp 105−107 °C; $[\alpha]_D^{24}$ +34(c 0.5, EtOH); ^{1}H NMR (500 MHz, $CDCl_3$): δ = 4.57 (dd, J = 11.3, 1.4 Hz, 1H), 3.90−4.10 (m, 4H), 2.27(dq, J = 12.2, 6.9 Hz, 1H), 1.94−1.88 (m, 1H), 1.84 (d, J = 1.0 Hz, 3H), 1.86−1.80 (m, 1H), 1.79−1.73 (m, 2H), 1.72−1.65 (m, 1H), 1.62−1.42 (m, 4H), 1.22 (d, J = 6.9 Hz, 3H), 1.17 (s, 3H); ^{13}C NMR (125 MHz, $CDCl_3$): δ = 178.5, 137.3, 127.1, 108.1, 82.5, 65.7, 64.7, 53.1, 41.2, 41.1, 37.4, 37.2, 29.3, 24.8, 24.6, 12.4, 11.4; IR (KBr): 2940, 2870, 1773, 1659, 1457, 1380, 1308, 1244, 1172, 1143, 1087, 1065, 1023 cm^{-1}; Anal. Calcd for $C_{17}H_{24}O_4$: C, 69.84; H, 8.27. Found: C, 69.78; H, 8.26.

Preparation of Ketal 12. Ketal **10** (234 mg, 0.8 mmol) was dissolved in anhydrous THF (25 mL), and lithium aluminum hydride (30 mg, 0.8 mmol) was added to the solution. After the mixture stirred for 1 h at room temperature, a saturated aqueous solution of sodium sulfate was added cautiously until a thick white precipitate was formed. The precipitate was filtered off, and the solvent was evaporated to dryness. The crude reduction product **11** was dissolved in dry pyridine (6 mL), and pivalic anhydride (0.6 mL) was added. The mixture was kept at room temperature until all diol **11** disappeared (14 days) and then was diluted with water and extracted with diethyl ether. The organic layer was dried over Na_2SO_4, and the solvent was evaporated. The residual pyridine was removed by evaporation with toluene. The crude reaction mixture was chromatographed (13% ethyl acetate in hexanes) yielding pivalate **12** (222 mg, 73% based on **10**).

Colorless crystals, mp 127−128 °C; $[\alpha]_D^{24}$ +54 (c 0.5, EtOH); ^{1}H NMR (500 MHz, $CDCl_3$): δ = 4.36 (dd, J = 11.0, 4.1 Hz, 1H), 4.10−3.92 (m, 6H), 2.49−2.41 (m, 1H), 1.91 (s, 3H), 1.82−1.70 (m, 4H), 1.59−1.43 (m, 5H), 1.33−1.24 (m, 1H), 1.20 (s, 9H), 1.10 (s, 3H), 0.92 (d, J = 7.0 Hz, 3H). ^{13}C NMR (125 MHz, $CDCl_3$): δ = 178.6, 145.4, 126.3, 109.3, 72.8, 68.1, 65.5, 64.7, 46.6, 41.3, 38.8, 37.6, 36.8, 31.5, 29.3, 27.2, 23.6, 20.5, 12.2, 10.8. IR ($CDCl_3$): 3623, 2959, 1718, 1459, 1288, 1157, 1074 cm^{-1}; Anal. Calcd for $C_{22}H_{36}O_5$: C, 69.44; H, 9.53. Found: C, 69.45; H, 9.60.

Preparation of Enone 1. A solution of **12** (115 mg, 0.3 mmol) in pyridine (3 mL) was added to the complex prepared by the addition of chromium trioxide (200 mg, 2 mmol) to pyridine (3 mL) at 0 °C. The mixture was stirred at room temperature for 20 h, and then diethyl ether was added (20 mL). The solids were filtered off, and the solvent was evaporated. The residual pyridine was removed by evaporation with toluene. The crude reaction mixture was chromatographed (10% ethyl acetate in hexanes) yielding enone **1** (94 mg, 82%).

Colorless crystals, mp 63−65 °C; $[\alpha]_D^{24}$ +59 (c 0.5, EtOH); ^{1}H NMR (500 MHz, $CDCl_3$): δ = 4.10−4.04 (m, 2H), 4.03−3.92 (m, 4H), 2.58−2.50 (m, 1H), 2.43−2.36 (m, 1H), 1.94−1.86 (m, 1H), 1.83−1.69 (m, 6H), 1.63 (s, 3H), 1.62−1.56 (m, 1H), 1.19 (s, 9H), 0.98 (s, 3H), 0.94 (d, J = 6.9 Hz, 3H); ^{13}C NMR (125 MHz, $CDCl_3$): δ = 206.5, 178.4, 145.2, 133.9, 107.2, 67.3, 65.9, 64.9, 53.2, 39.9, 38.9, 38.8, 35.6, 30.8, 29.3, 27.2, 23.0, 22.7, 13.01, 12.97; IR (KBr): 2952, 1721, 1681, 1479, 1287, 1173 cm^{-1}; Anal. Calcd for $C_{22}H_{34}O_5$: C, 69.81; H, 9.05. Found: C, 69.98; H, 9.13.

Preparation of 13. Dihydrosantonin (**6**, 580 mg, 2.3 mmol) was dissolved in anhydrous THF (60 mL), and lithium tri-*tert*-butoxyaluminum hydride (1.2 g, 4.7 mmol) was added to the solution. After the mixture stirred for 2 h at room temperature, a saturated aqueous solution of sodium sulfate was added cautiously until a thick white precipitate was formed. The precipitate was filtered off, and the solvent was evaporated to dryness. The residue was chromatographed (15% acetone in hexanes) yielding a mixture of stereomers **13** (equatorial/axial = 17:3) (560 mg, 95%). An analytical sample of pure equatorial isomer was prepared by crystallization from methanol.

Colorless crystals, mp 99−100 °C; $[\alpha]_D^{24}$ −26 (c 0.5, EtOH); ^{1}H NMR (500 MHz, $CDCl_3$): δ = 4.60 (d, J = 11.1 Hz, 1H), 4.01−3.95 (m, 1H), 2.28 (dq, J = 12.2, 6.9 Hz, 1H), 1.96 (s, 3H), 1.93−1.85 (m, 2H), 1.72 (qd, J = 11.8, 3.4 Hz, 1H), 1.67−1.59 (m, 4H), 1.52−1.49 (m, 1H), 1.48−139 (m, 2H), 1.23 (d, J = 6.9 Hz, 3H), 1.18 (s, 3H); ^{13}C NMR (125 MHz, $CDCl_3$): δ = 178.6, 133.8, 128.1, 82.7, 71.5, 53.6, 41.3, 40.6, 37.8, 36.4, 28.2, 26.2, 24.6, 15.5, 12.4; IR ($CHCl_3$): 3611, 2936, 1769, 1457, 1380, 1139, 1030 cm^{-1}; Anal. Calcd for $C_{15}H_{22}O_3$: C, 71.97; H, 8.86. Found: C, 71.89; H, 8.93.

Preparation of 14. A mixture of **13** (500 mg, 2.5 mmol), *tert*-butyldimethylchlorosilane (450 mg, 3 mmol), dichloromethane (6 mL), triethylamine (0.6 mL), and DMAP (50 mg, 0.4 mmol) was kept at room temperature for 20 h and then diluted with dichloromethane (50 mL) and washed with water. The organic layer was dried over Na_2SO_4, and the solvent was evaporated to dryness. The residue was chromatographed (5% ethyl acetate in hexanes) yielding **14** (610 mg, 84%) as a mixture of equatorial/axial isomers in a ratio of 17:3. The mixture was crystallized from methanol/water affording pure equatorial isomer **14** (480 mg, 66%).

Colorless crystals, mp 107−108 °C; $[\alpha]_D^{24}$ −7 (c 0.5, EtOH); ^{1}H NMR (500 MHz, $CDCl_3$): δ = 4.56 (d, J = 11.2 Hz, 1H), 3.99−3.95 (m, 1H), 2.25 (dq, J = 12.1, 6.9 Hz, 1H), 1.91−1.85 (m, 1H), 1.87 (s, 3H), 1.80−1.47 (m, 6H), 1.44−1.33 (m, 2H), 1.21 (d, J = 6.9 Hz, 3H), 1.17 (s, 3H), 0.90 (s, 9H), 0.09 (s, 3H), 0.07 (s, 3H); ^{13}C NMR (125 MHz, $CDCl_3$): δ = 178.7, 132.3, 129.4, 82.9, 72.3, 53.6, 41.3, 41.1, 37.7, 36.9, 28.8, 26.0, 25.9, 24.7, 18.1, 15.6, 12.4, −4.2, −4.7; IR ($CHCl_3$): 2932, 1768, 1460, 1379, 1360, 1330, 1255, 1057, 1031 cm^{-1}; Anal. Calcd for $C_{21}H_{36}O_3Si$: C, 69.18; H, 9.95. Found: C, 69.08; H, 9.85.

Preparation of 16. Sillyl ether **14** (400 mg, 1.1 mmol) was dissolved in anhydrous THF (25 mL) and lithium aluminum hydride (50 mg, 1.3 mmol) was added to the solution. After stirring for 1 h at room temperature, saturated aqueous solution of sodium sulfate was added cautiously until a thick white precipitate was formed. The precipitate was filtered off and the solvent was evaporated to dryness. The crude reduction product **15** was dissolved in dry pyridine (8 mL) and pivalic anhydride (2 mL) was added. The mixture was kept at room temperature until all diol **15** disappeared (14 days) and then diluted with water and extracted with diethyl ether. The organic layer was dried over Na_2SO_4 and the solvent was evaporated. The residual pyridine was removed by evaporation with toluene. The crude reaction mixture was chromatographed (10% ethyl acetate and 0.1% Et_3N in hexanes) yielding pivalate **16** (353 mg, 71% based on **14**).

Colorless oil, $[\alpha]_D^{24}$ +14 (c 0.5, EtOH); ^{1}H NMR (500 MHz, $CDCl_3$): δ = 4.35 (d, J = 11.0 Hz, 1H), 4.02−3.91 (m, 3H), 2.50−2.41 (m, 1H), 1.95 (s, 3H), 1.83−1.67 (m, 3H), 1.58−1.39 (m, 6H), 1.25 (dt, J = 12.7, 2.3 Hz, 1H), 1.20 (s, 9H), 1.10 (s, 3H), 0.92 (d, J = 8.2 Hz, 3H), 0.91 (s, 9H), 0.10 (s, 3H), 0.09 (s, 3H); ^{13}C NMR (125 MHz, $CDCl_3$): δ = 178.6, 140.3, 128.8, 74.4, 72.8, 68.2, 46.8, 41.6, 38.8, 37.8, 36.9, 31.5, 29.0, 27.2, 26.0, 24.6, 20.6, 18.2, 17.1, 10.8, −4.1, −4.7; IR ($CHCl_3$): 3620, 2933, 2857, 1718, 1461, 1288, 1156, 1080, 1050 cm^{-1}; HRMS (ESI) m/z: [M + Na]$^+$ Calcd for $C_{26}H_{48}O_4NaSi$ 475.3220; Found: 475.3217.

Preparation of 2. A solution of **16** (190 mg, 0.4 mmol) in pyridine (4 mL) was added to the complex prepared by the addition of chromium trioxide (300 mg, 3 mmol) to pyridine (6 mL) at 0 °C. The mixture was stirred at room temperature for 20 h, and then diethyl

DOI: 10.1021/acs.joc.6b00416
J. Org. Chem. XXXX, XXX, XXX−XXX

ether was added (30 mL). The solids were filtered off and washed with diethyl ether, and the solvent was evaporated. The residual pyridine was removed by evaporation with toluene. The crude reaction mixture was chromatographed (2% ethyl acetate in hexanes) yielding enone **2** (143 mg, 75%).

Colorless crystals, mp 85−87 °C; $[\alpha]_D^{24}$ +9 (*c* 0.3, EtOH); ^{1}H NMR (500 MHz, $CDCl_3$): δ = 4.07 (dd, *J* = 9.1, 5.8 Hz, 1H), 4.01−3.94 (m, 2H), 2.63−2.55 (m, 1H), 2.32 (ddd, *J* = 12.4, 6.4, 4.1 Hz, 1H), 1.90−1.73 (m, 3H), 1.67 (s, 3H), 1.72−1.56 (m, 4H), 1.53 (dd, *J* = 13.3, 2.6 Hz, 1H), 1.19 (s, 9H), 0.99 (s, 3H), 0.93 (d, *J* = 6.9 Hz, 3H), 0.89 (s, 9H), 0.09 (s, 3H), 0.08 (s, 3H); ^{13}C NMR (125 MHz, $CDCl_3$): δ = 206.1, 178.4, 140.6, 138.7, 72.0, 67.4, 53.2, 40.3, 38.8, 38.7, 36.3, 30.8, 28.8, 27.2, 25.8, 24.7, 22.3, 18.1, 17.2, 12.9, −4.1, −4.9; IR ($CHCl_3$): 2957, 2930, 1717, 1689, 1623, 1604, 1461, 1286, 1164, 1092 cm^{-1}; Anal. Calcd for $C_{26}H_{46}O_4Si$: C, 69.28; H, 10.28. Found: C, 69.31; H, 10.40.

Preparation of 3. Tetrabutylammonium fluoride trihydrate (190 mg, 0.6 mmol) was added to a solution of **2** (84 mg, 0.19 mmol) in THF (4 mL), and the mixture was stirred at 40 °C for 2 h. Then water (20 mL) was added, and the mixture was extracted with diethyl ether. The organic layer was dried over Na_2SO_4 and evaporated to dryness. The residue was chromatographed (15% acetone in hexanes) yielding pure **3** (59 mg, 94%).

Colorless crystals, mp 58−60 °C, $[\alpha]_D^{24}$ +59 (*c* 0.5, EtOH); ^{1}H NMR (500 MHz, $CDCl_3$): δ = 4.10−3.95 (m, 3H), 2.62 (m, 1H), 2.34 (ddd, *J* = 12.3, 6.5, 2.2 Hz, 1H), 2.03−1.95 (m, 1H), 1.93−1.86 (m, 1H), 1.76 (s, 3H), 1.84−1.60 (m, 6H), 1.56 (qd, *J* = 13.6, 2.7 Hz, 1H), 1.19 (s, 9H), 1.00 (s, 3H), 0.94 (d, *J* = 6.9 Hz, 3H). ^{13}C NMR (125 MHz, $CDCl_3$): δ = 206.3, 178.4, 141.8, 137.0, 71.3, 67.3, 53.2, 40.0, 38.9, 38.8, 35.9, 30.8, 28.4, 27.2, 24.7, 22.4, 16.6, 12.9; IR ($CHCl_3$): 3596, 2968, 2937, 1720, 1688, 1626, 1480, 1457, 1381, 1286, 1164, 1032 cm^{-1}; HRMS (ESI) *m*/*z*: [M + Na]$^+$ Calcd for $C_{20}H_{32}O_4Na$ 359.2198; Found: 359.2204.

Preparation of 4. Mother liquors remaining after crystallization of **14** (120 mg, 0.26 mmol) were processed the same way as it was applied for **15** and **16** affording a mixture of isomers **4** and **2**. Pure component **4** (44 mg) was isolated by preparative TLC chromatography (10% diethyl ether in hexanes, three developments).

Colorless oil, $[\alpha]_D^{24}$ +60 (*c* 0.5, EtOH); ^{1}H NMR (500 MHz, $CDCl_3$): δ = 4.03−3.95 (m, 2H), 3.93−3.90 (m, 1H), 2.60−2.50 (m, 1H), 2.44−2.37 (m, 1H), 1.92−1.84 (m, 1H), 1.82−1.70 (m, 3H), 1.69 (s, 3H), 1.68−1.60 (m, 3H), 1.39−1.34 (m, 1H), 1.18 (s, 9H), 0.94 (d, *J* = 6.9 Hz, 3H), 0.91 (s, 3H), 0.89 (s, 9H), 0.08 (s, 6H); ^{13}C NMR (125 MHz, $CDCl_3$): δ = 207.9, 178.4, 141.9, 135.6, 69.1, 67.5, 53.1, 39.9, 38.9, 38.8, 32.7, 30.8, 27.9, 27.2, 25.8, 23.4, 22.6, 22.3, 18.0, 17.7, 13.1, −4.4, −4.7; IR ($CHCl_3$): 2956, 2932, 2857, 1731, 1693, 1638, 1472, 1467, 1283, 1254, 1162, 1079, 1032 cm^{-1}; HRMS (ESI) *m*/*z*: [M + Na]$^+$ Calcd for $C_{26}H_{46}O_4NaSi$ 473.3063; Found: 473.3066.

Preparation of 5. Tetrabutylammonium fluoride trihydrate (70 mg, 0.22 mmol) was added to a solution of **4** (28 mg, 0.06 mmol) in THF (2 mL), and the mixture was stirred at room temperature for 2 h. Then water (20 mL) was added, and the mixture was extracted with diethyl ether. The organic layer was dried over Na_2SO_4 and evaporated to dryness. The residue was chromatographed (15% acetone in hexanes) yielding pure **5** (15 mg, 71%).

Pale yellow oil, $[\alpha]_D^{24}$ +96 (*c* 0.4, EtOH); ^{1}H NMR (600 MHz, $CDCl_3$): δ = 4.00−3.97 (m, 3H), 2.61−2.54 (m, 1H), 2.42−2.37 (m, 1H), 1.81 (s, 3H), 1.93−1.61 (m, 8H), 1.46 (dt, *J* = 13.0, 3.5 Hz, 1H), 1.19 (s, 9H), 0.95 (d, *J* = 6.9 Hz, 3H), 0.94 (s, 3H); ^{13}C NMR (150 MHz, $CDCl_3$): δ = 207.1, 178.5, 142. 8, 135.1, 68.5, 67.3, 53.1, 39.9, 38.9, 32.4, 30.7, 27.3, 27.23, 27.20, 23.1, 22.1, 18.0, 13.0; IR ($CHCl_3$): 3445, 2960, 2934, 2873, 1728, 1685, 1631, 1479, 1457, 1398, 1377, 1284, 1162, 1031 cm^{-1}; HRMS (ESI) *m*/*z*: [M + Na]$^+$ Calcd for $C_{20}H_{32}O_4Na$ 359.2198; Found: 359.2195.

Preparation of Dihydro-6-episantonin 7. Dihydrosantonin **6** (70 mg, 0.28 mmol) was dissolved in anhydrous DMF containing 5% HCl (1 mL), and the solution was heated at 80 °C for 1 h. Then the solution was diluted with water and extracted with diethyl ether. The organic layer was washed with water, saturated sodium bicarbonate, and brine. The organic portion was dried over Na_2SO_4 and evaporated to dryness. The residue was chromatographed (20% ethyl acetate in hexanes) yielding **7** (57 mg, 81%) as colorless crystals.

Colorless crystals, mp 123−124 °C (lit.[31] 125 °C), $[\alpha]_D^{24}$ −137 (*c* 0.4, EtOH); ^{1}H NMR (500 MHz, $CDCl_3$): δ = 5.45 (d, *J* = 5.3 Hz, 1H), 2.71 (ddd, *J* = 17.9, 14.9, 5.5 Hz, 1H), 2.53−2.48 (m, 2H), 2.21 (dt, *J* = 10.8, 5.8 Hz, 1H), 1.91 (s, 3H), 1.94−1.86 (m, 1H), 1.79−1.70 (m, 2H), 1.66−1.56 (m, 2H), 1.39 (d, *J* = 7.7 Hz, 3H), 1.41−1.37 (m, 1H), 1.26 (s, 3H); ^{13}C NMR (125 MHz, $CDCl_3$): δ = 198.8, 179.5, 151.2, 136.6, 75.8, 43.7, 43.1, 37.8, 37.7, 34.4, 34.0, 23.8, 23.1, 15.1, 10.8; IR ($CHCl_3$): 2973, 2938, 2871, 1767, 1670, 1455, 1380, 1317, 1160, 957 cm^{-1}; Anal. Calcd for $C_{15}H_{20}O_3$: C, 72.55; H, 8.12. Found: C, 72.83; H, 8.03.

Crystallization of dihydroepisantonin (**7**) from the mixture of methanol/water 1:1 led to needle-like crystals: mp 96−98 °C; IR (KBr): 2973, 2942, 2921, 2867,1773, 1669, 1645, 1590,1453, 1381, 1361, 1329, 1312, 1214, 1199, 1161, 1069, 1024, 953, 932 cm^{-1}.

Crystallization of dihydroepisantonin (**7**) from hexane gave prismatic crystals: mp 123−124 °C; IR (KBr): 2940, 1874, 792, 1767, 1675, 1622, 1454, 1331, 1291, 1238, 1209, 1185, 1138, 1099, 1028, 985 cm^{-1}.

Preparation of Ketoester 8. A mixture of zinc dust (350 mg, 5.4 mmol), dihydro-6-episantonin **7** (120 mg, 0.5 mmol), anhydrous AcOH (0.08 mL), and anhydrous methanol (3.0 mL) was heated at 60 °C in an oil bath for 40 min. Then the reaction mixture was cooled to room temperature and directly treated with an excess of ethereal diazomethane, until the persistence of a pale yellow color. The mixture was then filtered, and the solvents were removed in *vacuo*. A dry oily residue was chromatographed (10% ethyl acetate in hexanes) to yield ester **8** (114 mg, 89%) as a colorless oil.

$[\alpha]_D^{24}$ +117 (*c* 0.4, MeOH) [lit.[78] $[\alpha]_D^{23}$ +115 (*c* 0.2, MeOH)]; ^{1}H NMR (500 MHz, $CDCl_3$): δ = 3.71 (s, 3H), 2.65−2.60 (m, 1H), 2.50 (ddd, *J* = 16.9, 13.4, 6.2 Hz, 1H), 2.44−2.36 (m, 2H), 1.90 (t, *J* = 13.1 Hz, 1H), 1.82−1.65 (m, 5H), 1.74 (d, *J* = 1.1 Hz, 3H), 1.50−1.36 (m, 2H), 1.20 (d, *J* = 6.8 Hz, 3H), 1.19 (s, 3H); ^{13}C NMR (125 MHz, $CDCl_3$): δ = 198.0, 176.1, 161.3, 128.8, 51.5, 45.1, 41.5, 41.3, 37.3, 35.8, 33.7, 32.0, 24.6, 22.3, 14.0, 10.7; IR ($CHCl_3$): 2927, 2860, 1735, 1666, 1612, 1455, 1435, 1375, 1349, 1192, 1166, 1065 cm^{-1}; HRMS (ESI) *m*/*z*: [M + Na]$^+$ Calcd for $C_{16}H_{24}O_3Na$ 287.1623; Found: 287.1614.

■ ASSOCIATED CONTENT

Supporting Information

The Supporting Information is available free of charge on the ACS Publications website at DOI: 10.1021/acs.joc.6b00416.

Crystallographic data for **1** (CIF)
Crystallographic data for **3** (CIF)
Crystallographic data for **6** (CIF)
Crystallographic data for **7**, needle-like crystals (CIF)
Crystallographic data for **7**, prism-like crystals (CIF)
^{1}H NMR, ^{13}C NMR, and IR spectra for compounds **1**−**15** and details of computational studies (PDF)

■ AUTHOR INFORMATION

Corresponding Authors

*E-mail: jadwiga.frelek@icho.edu.pl.
*E-mail: grimme@thch.uni-bonn.de.

Notes

The authors declare no competing financial interest.

■ ACKNOWLEDGMENTS

This work was supported by Grant No. UMO-2011/01/B/ST5/06413 from the National Science Centre of Poland. The GAUSSIAN calculations were performed at the Interdisciplinary Centre for Mathematical and Computational Modeling (ICM) of University of Warsaw (Grant Nos. G34-15 and G36-

DOI: 10.1021/acs.joc.6b00416
J. Org. Chem. XXXX, XXX, XXX−XXX

12). C.B. thanks Jakob Seibert for his help concerning the sTD-DFT calculations on the MD trajectories.

REFERENCES

(1) Ndi, C. P.; Semple, S. J.; Griesser, H. J.; Pyke, S. M.; Barton, M. D. *J. Nat. Prod.* **2007**, *70*, 1439−1443.
(2) Pasikanti, S.; Reddy, D. S.; Iqbal, J.; Dubey, P. K.; Das, P. *Synthesis* **2009**, *2009*, 3833−3837.
(3) Barr, A. *Traditional Bush Medicines: An Aboriginal Pharmacopoeia. Aboriginal Communities of the Northern Territory of Australia*; Greenhouse Publications: Richmond, Victoria, 1988.
(4) McMorris, T. C.; Kelner, M. J.; Wang, W.; Estes, L. A.; Montoya, M. A.; Taetle, R. *J. Org. Chem.* **1992**, *57*, 6876−6883.
(5) Harada, N.; Nakanishi, K. *J. Chem. Soc. D* **1970**, 310−311.
(6) Matsuo, A. *Tetrahedron* **1972**, *28*, 1203−1209.
(7) Djerassi, C.; Records, R.; Bunnenberg, E.; Mislow, K.; Moscowitz, A. *J. Am. Chem. Soc.* **1962**, *84*, 870−872.
(8) Whalley, W. B. *Chem. Ind.* **1962**, 1024−1027.
(9) Snatzke, G. *Optical Rotatory Dispersion and Circular Dichroism in Organic Chemistry*; Sadtler Research Labs Inc.: Philadelphia, 1967.
(10) Burgstahler, A. W.; Barkhurst, R. C. *J. Am. Chem. Soc.* **1970**, *92*, 7601−7603.
(11) Kirk, D. N. *Tetrahedron* **1986**, *42*, 777−818.
(12) Gawronski, J. K. *Tetrahedron* **1982**, *38*, 3−26.
(13) Gawronski, J. K. In *The Chemistry of Enones*; Patai, S., Rappoport, Z., Eds.; John Wiley & Sons Ltd: New York, 1989; pp 55−105.
(14) Kwit, M.; Gawronski, J. K.; Boyd, D. R.; Sharma, N. D.; Kaik, M. *Org. Biomol. Chem.* **2010**, *8*, 5635−5645.
(15) Kwit, M.; Skowronek, P.; Gawronski, J.; Frelek, J.; Woznica, M.; Butkiewicz, A. In *Comprehensive Chiroptical Spectroscopy*; Berova, N., Polavarapu, P. L., Nakanishi, K., Woody, R. W., Eds.; John Wiley&Sons, Inc., Publication: Hoboken, New Jersey, 2012; Vol. *2*, pp 39−51.
(16) Frelek, J.; Szczepek, W. J.; Weiss, H. P.; Reiss, G. J.; Frank, W.; Brechtel, J.; Schultheis, B.; Kuball, H.-G. *J. Am. Chem. Soc.* **1998**, *120*, 7010−7019.
(17) Diedrich, C.; Grimme, S. *J. Phys. Chem. A* **2003**, *107*, 2524−2539.
(18) Frelek, J.; Szczepek, W. J.; Weiss, H. P. *Tetrahedron: Asymmetry* **1995**, *6*, 1419−1430.
(19) Frelek, J.; Szczepek, W. J.; Weiss, H. P. *Tetrahedron: Asymmetry* **1993**, *4*, 411−424.
(20) Frelek, J.; Szczepek, W. J.; Neubrecht, S.; Schultheis, B.; Brechtel, J.; Kuball, H.-G. *Chem. - Eur. J.* **2002**, *8*, 1899−1907.
(21) Chochrek, P.; Frelek, J.; Kwit, M.; Wicha, J. *J. Org. Chem.* **2009**, *74*, 7300−7308.
(22) Woznica, M.; Butkiewicz, A.; Grzywacz, A.; Kowalska, P.; Masnyk, M.; Michalak, K.; Luboradzki, R.; Furche, F.; Kruse, H.; Grimme, S.; Frelek, J. *J. Org. Chem.* **2011**, *76*, 3306−3319.
(23) Polavarapu, P. L.; Frelek, J.; Woznica, M. *Tetrahedron: Asymmetry* **2011**, *22*, 1720−1724.
(24) Gorecki, M.; Suszczynska, A.; Woznica, M.; Baj, A.; Wolniak, M.; Cyranski, M.; Witkowski, S.; Frelek, J. *Org. Biomol. Chem.* **2014**, *12*, 2235−2254.
(25) Krohn, K.; Kouam, S. F.; Kuigoua, G. M.; Hussain, H.; Cludius-Brandt, S.; Flörke, U.; Kurtán, T.; Pescitelli, G.; Di Bari, L.; Draeger, S.; Schulz, B. *Chem. - Eur. J.* **2009**, *15*, 12121−12132.
(26) Di Bari, L.; Pescitelli, G.; Salvadori, P.; Rovini, M.; Anzini, M.; Cappelli, A.; Vomero, S. *Tetrahedron: Asymmetry* **2006**, *17*, 3430−3436.
(27) Frelek, J.; Karchier, M.; Madej, D.; Michalak, K.; Różański, P.; Wicha, J. *Chirality* **2014**, *26*, 300−306.
(28) Hans, M.; Charpentier, M.; Huch, V.; Jauch, J.; Bruhn, T.; Bringmann, G.; Quandt, D. *J. Nat. Prod.* **2015**, *78*, 2381−2389.
(29) Gehrold, A. C.; Bruhn, T.; Bringmann, G. *J. Org. Chem.* **2016**, *81*, 1075−1088.
(30) Kang, T.; Kim, Y.; Lee, D.; Wang, Z.; Chang, S. *J. Am. Chem. Soc.* **2014**, *136*, 4141−4144.
(31) Greene, A. E.; Muller, J.-C.; Ourisson, G. *J. Org. Chem.* **1974**, *39*, 186−191.
(32) Gulge, R. *Indian J. Chem.* **1986**, *25B*, 180−182.
(33) Marco, J. A.; Arno, M.; Carda, M. *Can. J. Chem.* **1987**, *65*, 630−635.
(34) Frelek, J.; Górecki, M.; Łaszcz, M.; Suszczyńska, A.; Vass, E.; Szczepek, W. J. *Chem. Commun.* **2012**, *48*, 5295−5297.
(35) Górecki, M. *Chirality* **2015**, *27*, 441−448.
(36) Lightner, D. A.; Gurst, J. E. *Organic Conformational Analysis and Stereochemistry from Circular Dichroism Spectroscopy*; Wiley-VCH: New York, 2000.
(37) Beecham, A. F. *Tetrahedron* **1971**, *27*, 5207−5216.
(38) Kuball, H.-G.; Altschuh, J.; Kulbach, K.; Schoenhofer, A. *Helv. Chim. Acta* **1978**, *61*, 571−588.
(39) Kuball, H.-G.; Acimis, M.; Altschuh, J. *J. Am. Chem. Soc.* **1979**, *101*, 20−27.
(40) Kuball, H.-G.; Schultheis, B.; Klasen, M.; Frelek, J.; Schönhofer, A. *Tetrahedron: Asymmetry* **1993**, *4*, 517−528.
(41) Kundrat, M. D.; Autschbach, J. *J. Am. Chem. Soc.* **2008**, *130*, 4404−4414.
(42) Nitsch-Velasquez, L.; Autschbach, J. *Chirality* **2010**, *22*, E81−E95.
(43) Dierksen, M.; Grimme, S. *J. Chem. Phys.* **2004**, *120*, 3544−3554.
(44) *CONFLEX 7*; Conflex corporation.
(45) Frisch, M. J.; Trucks, G. W.; Schlegel, H. B.; Scuseria, G. E.; Robb, M. A.; Cheeseman, J. R.; Scalmani, G.; Barone, V.; Mennucci, B.; Petersson, G. A.; Nakatsuji, H.; Caricato, M.; Li, X.; Hratchian, H. P.; Izmaylov, A. F.; Bloino, J.; Zheng, G.; Sonnenberg, J. L.; Hada, M.; Ehara, M.; Toyota, K.; Fukuda, R.; Hasegawa, J.; Ishida, M.; Nakajima, T.; Honda, Y.; Kitao, O.; Nakai, H.; Vreven, T.; Montgomery, J. A. J.; Peralta, J. E.; Ogliaro, F.; Bearpark, M.; Heyd, J. J.; Brothers, E.; Kudin, K. N.; Staroverov, V. N.; Kobayashi, R.; Normand, J.; Raghavachari, K.; Rendell, A.; Burant, J. C.; Iyengar, S. S.; Tomasi, J.; Cossi, M.; Rega, N.; Millam, J. M.; Klene, M.; Knox, J. E.; Cross, J. B.; Bakken, V.; Adamo, C.; Jaramillo, J.; Gomperts, R.; Stratmann, R. E.; Yazyev, O.; Austin, A. J.; Cammi, R.; Pomelli, C.; Ochterski, J. W.; Martin, R. L.; Morokuma, K.; Zakrzewski, V. G.; Voth, G. A.; Salvador, P.; Dannenberg, J. J.; Dapprich, S.; Daniels, A. D.; Farkas, Ö.; Foresman, J. B.; Ortiz, J. V.; Cioslowski, J.; Fox, D. J., *Gaussian 09*; Gaussian, Inc.
(46) Junior, F. M. S.; Covington, C. L.; de Amorim, M. B.; Velozo, L. S. M.; Kaplan, M. A. C.; Polavarapu, P. L. *J. Nat. Prod.* **2014**, *77*, 1881−1886.
(47) Grimme, S.; Brandenburg, J. G.; Bannwarth, C.; Hansen, A. *J. Chem. Phys.* **2015**, *143*, 054107.
(48) Grimme, S.; Antony, J.; Ehrlich, S.; Krieg, H. *J. Chem. Phys.* **2010**, *132*, 154104.
(49) Grimme, S.; Ehrlich, S.; Goerigk, L. *J. Comput. Chem.* **2011**, *32*, 1456−1465.
(50) Kruse, H.; Grimme, S. *J. Chem. Phys.* **2012**, *136*, 154101.
(51) Ahlrichs, R.; Bär, M.; Häser, M.; Horn, H.; Kölmel, C. *Chem. Phys. Lett.* **1989**, *162*, 165−169.
(52) Ahlrichs, R.; Armbruster, M. K.; Bachorz, R. A.; Bär, M.; Baron, H. P.; Bauernschmitt, R.; Bischoff, F. A.; Böcker, S.; Crawford, N.; Deglmann, P.; Della Sala, F.; Diedenhofen, M.; Ehrig, M.; Eichkorn, K.; Elliott, S.; Friese, D.; Furche, F.; Glöß, A.; Haase, F.; Häser, M.; Hättig, C.; Hellweg, A.; Höfener, S.; Horn, H.; Huber, C.; Huniar, U.; Kattannek, M.; Klopper, W.; Köhn, A.; Kölmel, C.; Kollwitz, M.; May, K.; Nava, P.; Ochsenfeld, C.; Öhm, H.; Pabst, M.; Patzelt, H.; Rappoport, D.; Rubner, O.; Schäfer, A.; Schneider, U.; Sierka, M.; Tew, D. P.; Treutler, O.; Unterreiner, B.; von Arnim, M.; Weigend, F.; Weis, P.; Weiss, H.; Winter, N. *TURBOMOLE*, V7.0 2015; a development of University of Karlsruhe and Forschungszentrum Karlsruhe GmbH, 1989−2007, TURBOMOLE GmbH, since 2007; available from http://www.turbomole.com.
(53) Zhao, Y.; Truhlar, D. G. *J. Phys. Chem. A* **2005**, *109*, 5656−5667.
(54) Weigend, F.; Furche, F.; Ahlrichs, R. *J. Chem. Phys.* **2003**, *119*, 12753−12762.

DOI: 10.1021/acs.joc.6b00416
J. Org. Chem. XXXX, XXX, XXX−XXX

(55) Weigend, F.; Ahlrichs, R. *Phys. Chem. Chem. Phys.* **2005**, *7*, 3297−3305.
(56) Grimme, S. *Chem. - Eur. J.* **2012**, *18*, 9955−9964.
(57) Klamt, A. *J. Phys. Chem.* **1995**, *99*, 2224−2235.
(58) Eckert, F.; Klamt, A. *AIChE J.* **2002**, *48*, 369−385.
(59) Eckert, F.; Klamt, A. *COSMOtherm*, Version C3.0, Release 12.01; COSMOlogic GmbH & Co. KG: Leverkusen, Germany, 2012.
(60) Eichkorn, K.; Treutler, O.; Öhm, H.; Häser, M.; Ahlrichs, R. *Chem. Phys. Lett.* **1995**, *240*, 283−290.
(61) Eichkorn, K.; Weigend, F.; Treutler, O.; Ahlrichs, R. *Theor. Chem. Acc.* **1997**, *97*, 119−124.
(62) Lee, C.; Yang, W.; Parr, R. G. *Phys. Rev. B: Condens. Matter Mater. Phys.* **1988**, *37*, 785−789.
(63) Becke, A. D. *Phys. Rev. A: At., Mol., Opt. Phys.* **1988**, *38*, 3098−3100.
(64) Becke, A. D. *J. Chem. Phys.* **1993**, *98*, 1372−1377.
(65) Yanai, T.; Tew, D. P.; Handy, N. C. *Chem. Phys. Lett.* **2004**, *393*, 51−57.
(66) Schäfer, A.; Huber, C.; Ahlrichs, R. *J. Chem. Phys.* **1994**, *100*, 5829−5835.
(67) Grimme, S. *J. Chem. Phys.* **2013**, *138*, 244104.
(68) Risthaus, T.; Hansen, A.; Grimme, S. *Phys. Chem. Chem. Phys.* **2014**, *16*, 14408−14419.
(69) Bannwarth, C.; Grimme, S. *Comput. Theor. Chem.* **2014**, *1040*−*1041*, 45−53.
(70) Neese, F. *WIRES Comp. Mol. Sci.* **2012**, *2*, 73−78.
(71) Neese, F. *ORCA − An ab initio, Density Functional and Semiempirical Program Package*, Ver. 3.0; Max Planck Institute for Bioinorganic Chemistry: Germany, 2014.
(72) Klamt, A.; Schuurmann, G. *J. Chem. Soc., Perkin Trans. 2* **1993**, *5*, 799−805.
(73) Grimme, S. *J. Chem. Theory Comput.* **2014**, *10*, 4497−4514.
(74) Ryckaert, J. P.; Ciccotti, G.; Berendsen, H. J. *J. Comput. Phys.* **1977**, *23*, 327−341.
(75) van Gunsteren, W. F.; Berendsen, H. J. C. *Mol. Phys.* **1977**, *34*, 1311−1327.
(76) Shushkov, P.; Grimme, S. *QMSIM*, Version 1.0; Universität Bonn: 2015; http://www.thch.uni-bonn.de/tc/.
(77) Banerji, J. C.; Barton, D. H. R.; Cookson, R. C. *J. Chem. Soc.* **1957**, *0*, 5041−5050.
(78) Piers, E.; Cheng, K. F. *Can. J. Chem.* **1968**, *46*, 377−383.

DOI: 10.1021/acs.joc.6b00416
J. Org. Chem. XXXX, XXX, XXX−XXX